

# Journal of Materials Chemistry A

Accepted Manuscript



This is an *Accepted Manuscript*, which has been through the Royal Society of Chemistry peer review process and has been accepted for publication.

*Accepted Manuscripts* are published online shortly after acceptance, before technical editing, formatting and proof reading. Using this free service, authors can make their results available to the community, in citable form, before we publish the edited article. We will replace this *Accepted Manuscript* with the edited and formatted *Advance Article* as soon as it is available.

You can find more information about *Accepted Manuscripts* in the [Information for Authors](#).

Please note that technical editing may introduce minor changes to the text and/or graphics, which may alter content. The journal's standard [Terms & Conditions](#) and the [Ethical guidelines](#) still apply. In no event shall the Royal Society of Chemistry be held responsible for any errors or omissions in this *Accepted Manuscript* or any consequences arising from the use of any information it contains.



## ARTICLE

## Efficient Oxygen Reduction Reaction Electrocatalysts Synthesized from Iron-coordinated Aromatic Polymer Framework

Yong Zhao,<sup>ab</sup> Kazuhide Kamiya,<sup>b</sup> Kazuhito Hashimoto\*,<sup>b</sup> Shuji Nakanishi\*<sup>b</sup>

Received 00th January 20xx,  
Accepted 00th January 20xx

DOI: 10.1039/x0xx00000x

[www.rsc.org/](http://www.rsc.org/)

Aromatic polymer with abundant nitrogen-coordinated iron (Fe-N<sub>x</sub>) species provide a big chance to prepare iron-nitrogen co-doped carbon (Fe-N<sub>x</sub>/C) catalyst with highly efficient oxygen reduction reaction (ORR) activity, however, such type of materials have not been reported so far. Herein, we synthesized a metal-coordinated aromatic polymer, Fe<sup>(III)</sup>-poly(o-phenylene-diamine (Fe-PPDA)), with dense Fe-N<sub>x</sub> species by a facile route. Fe-PPDA was obtained by polymerization of o-phenylenediamine/ferric-ion complex in the presence of sodium bicarbonate, which was essential in retaining abundant Fe-N<sub>x</sub> species and increasing surface area of polymer. Fe-PPDA polymer derived Fe-N<sub>x</sub>/C catalysts demonstrated activity in ORRs, with onset and half-wave potentials (E<sub>1/2</sub>) of 1.11 V<sub>RHE</sub> and 0.92 V<sub>RHE</sub>, respectively, which were superior to the values obtained for commercial Pt/C (E<sub>1/2</sub>, 0.85 V<sub>RHE</sub>) and are the best values yet reported for the Fe-N<sub>x</sub>/C family in alkaline medium. It also demonstrated the comparable ORR activity to that of commercial Pt/C catalyst in acidic medium (E<sub>1/2</sub>, 0.76 V<sub>RHE</sub> vs 0.78 V<sub>RHE</sub>). The excellent ORR activity was ascribed to the abundant Fe-N<sub>x</sub>, modulated carbon nanostructure and the high surface area.

### Broader content

The preparation of highly-active and durable non-precious metal catalysts for oxygen reduction reaction (ORR) is highly important for reducing the cost of fuel cells. Transition metal and nitrogen codoped carbon (Fe-N<sub>x</sub>/C) materials are regarded as one of the most promising catalysts for the cathode materials of fuel cells. The ORR activity of Fe-N<sub>x</sub>/C materials is strongly dependent on the density of catalytic active sites and the effective surface area. In this article, we report a facile protocol to prepare Fe-N<sub>x</sub>/C materials with dense active sites and high surface area by using an iron-coordinated aromatic polymer as the starting precursor, which has abundant N-coordinated-Fe units in the metal-polymer framework. The results indicated that the ORR activity of Fe-N<sub>x</sub>/C materials was substantially promoted by using iron-coordinated polymer precursors compared with that synthesized from the physical mixture of iron salt and polymer in traditional method. The newly-developed Fe-N<sub>x</sub>/C catalysts exhibited much better and comparable ORR activity compared to that of commercial Pt/C catalysts in the alkaline and acidic medium, respectively.

### Introduction

Cost-effective oxygen reduction reaction (ORR) electrocatalysts are essential for the industrial application of various types of fuel cells and metal-air batteries.<sup>1-16</sup> Carbon materials co-doped with nitrogen and transition metals (M-N<sub>x</sub>/C)<sup>17-21</sup> have been widely studied as ORR catalysts because of their tunable electronic and spin structure in outer orbital, and advanced ORR activity and stability that resemble those of Pt-based precious metal catalysts.<sup>21,22</sup> Since polyacrylonitrile was firstly demonstrated as precursor to prepare M-N<sub>x</sub>/C material as ORR catalyst,<sup>23</sup> numerous N-contained polymers<sup>18,24-28</sup> were

exploited as starting materials to prepare M-N<sub>x</sub>/C catalysts. Among the family of N-contained polymers, aromatic polymer (for example, polyaniline and poly(phenylenediamine)) derived catalysts always showed the better activity and durability than catalysts derived from aliphatic amine, implying that the type of carbon nanostructure formed during pyrolysis might be one of the critical factors for catalyst performance.<sup>21</sup> Equally important, incorporation of N-coordinated Fe (Fe-N<sub>x</sub>) species into polymers can substantially improve the ORR activity of Fe-N<sub>x</sub>/C materials, demonstrating that Fe-N<sub>x</sub> species may modulate the carbon nanostructure and/or be direct active sites for ORR.<sup>24</sup> It implied that synthesis of aromatic polymer with dense and uniformly-dispersed Fe-N<sub>x</sub> species may have the big opportunity to obtain the efficient ORR catalysts.

Almost all aromatic-polymer derived Fe-N<sub>x</sub>/C catalysts were synthesized from pyrolysis of the mechanically mixed iron salts and nano-sized polymers.<sup>18,24-26</sup> Fe-N<sub>x</sub> species was only existed on polymer surface, and it was difficult to incorporate Fe-N<sub>x</sub> species into the bulk of polymer with this conventional method.<sup>21</sup> Bulk of polymer is exposed to be surface after pyrolysis treatment. The negligible amount of Fe-N<sub>x</sub> species in

<sup>a</sup>Key Lab for Special Functional Materials of Ministry of Education, Collaborative Innovation Center of Nano Functional Materials and Applications, Henan University, Kaifeng, 475004, Henan Province, P. R. China.

<sup>b</sup>Department of Applied Chemistry, The University of Tokyo 7-3-1 Hongo, Bunkyo-ku, Tokyo 113-8656, Japan. E-mail: [hashimoto@light.t.u-tokyo.ac.jp](mailto:hashimoto@light.t.u-tokyo.ac.jp); [nakanishi@light.t.u-tokyo.ac.jp](mailto:nakanishi@light.t.u-tokyo.ac.jp)

Electronic Supplementary Information (ESI) available: additional XPS spectra, XANES and EXAFS spectra, and electrochemical tests. See DOI: 10.1039/x0xx00000x

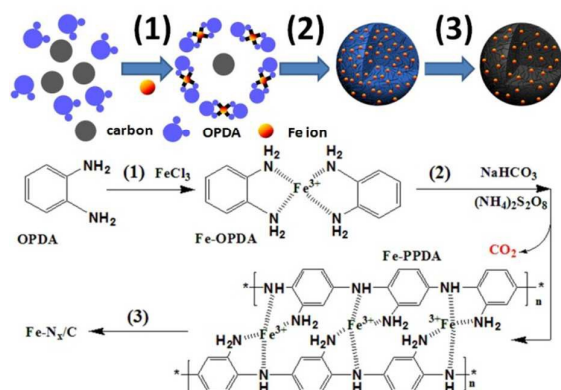


**Figure 1.** a) Schematic illustration of the synthetic process for Fe-N<sub>x</sub>/C-1. (1) formation of Fe-OPDA complex; (2) polymerization of Fe-OPDA in the presence of NaHCO<sub>3</sub> and (NH<sub>4</sub>)<sub>2</sub>S<sub>2</sub>O<sub>8</sub>; (3) pyrolysis of the Fe-PPDA-1 polymer and treatment of the pyrolyzed samples with HCl acid.

the bulk means that the modulation of carbon nanostructure by Fe-N<sub>x</sub> species and formation of dense Fe-N<sub>x</sub> species are not favored on the catalyst surface. Aromatic polymer with abundant Fe-N<sub>x</sub> species both in the bulk and on the surface can provide an opportunity to flexibly modulate carbon nanostructure by Fe-N<sub>x</sub> and achieve highly dense Fe-N<sub>x</sub> species on catalyst surface for enhancement of ORR activity.

In this work, we show a unique synthesis protocol to obtain iron-coordinated aromatic polymer, (Fe<sup>(III)</sup>-poly(*o*-phenylenediamine), Fe-PPDA), with high content of Fe-N<sub>4</sub> species. Fe-PPDA polymer was successfully synthesized by polymerization of *o*-phenylenediamine/ferric-ion complex in the presence of sodium bicarbonate, which was essential in retaining high content of Fe-N<sub>4</sub> species and increasing surface area of polymer. Experimental characterization revealed that Fe-N<sub>x</sub>/C materials possessed dense and mono-dispersed Fe-N<sub>x</sub> species, high ratio of quaternary-N to pyridinic-N, and big effective surface area, which were considered as the determined factors for their efficient ORR activity in both alkaline and acidic medium.

## Experimental

### Materials

ortho-phenylenediamine (OPDA), ferric chloride (FeCl<sub>3</sub>), sodium bicarbonate (NaHCO<sub>3</sub>), ammonium persulfate ((NH<sub>4</sub>)<sub>2</sub>S<sub>2</sub>O<sub>8</sub>), sodium sulfate (Na<sub>2</sub>SO<sub>4</sub>) were purchased from Wako Company, Japan. Ketjen carbon black (EC300J) was a gift from Mitsubishi chemical company. O<sub>2</sub> and Ar gas was purchased from Taiyo Nippon Sanso Corporation.

### The preparation of Fe-N<sub>x</sub>/C-1

The carbon particles (0.2 g) were ultrasonically dispersed in water solution with ultrasonic probe system. 0.01 mol OPDA (1.08 g) dissolved in distilled water was poured into above suspension and stirred with one hour. And then, 0.005 mol FeCl<sub>3</sub>·6H<sub>2</sub>O (1.35 g) was added into above suspension, and stirred for several minutes. A hybrid solution of 0.01 mol

(NH<sub>4</sub>)<sub>2</sub>S<sub>2</sub>O<sub>8</sub> (2.28 g) and 0.02 mol NaHCO<sub>3</sub> (1.68 g) was poured down to above suspension to polymerize the Fe-OPDA complex to form Fe-PPDA polymer. The pH value was kept constant at a value of 2.1 before and after polymerization of Fe-OPDA. The suspension was centrifuged and washed with distilled water three times to remove the soluble chemicals. The resulted wet-powder was ultrasonically dispersed in 100 ml distilled water, and then freeze-dried at -45 °C for 24 h to obtain the Fe-PPDA-1/C powder. The powder was pyrolyzed at 800 °C for 2 h under a temperature program (0-to-800 °C, 3 h; 800 °C, 2h; 800-to-0 °C, 3 h) in the tubular furnace. The pyrolyzed sample was treated with concentrated HCl solution for 8 h, followed by centrifugation and washing with distilled water three times. Finally, the obtained powder was dried at 60 °C.

### Fe-PPDA-1 polymer for EXAFS and XANS

The synthesis of Fe-PPDA-1 polymer was similar to that of Fe-PPDA-1/C materials, while no carbon particle was added.

### The preparation of Fe-N<sub>x</sub>/C-2

The synthesis procedure of Fe-N<sub>x</sub>/C-2 material was similar to that of Fe-N<sub>x</sub>/C-1, while no NaHCO<sub>3</sub> was added during the polymerization of Fe-OPDA. The calcinations procedure was the same as that of Fe-N<sub>x</sub>/C-1.

### The preparation of Fe-N<sub>x</sub>/C-3

0.01 mol OPDA dissolved in water was poured into the well-dispersed carbon suspension (0.2 g). A solution of 0.01 mol (NH<sub>4</sub>)<sub>2</sub>S<sub>2</sub>O<sub>8</sub> (2.28 g) was added into above suspension to polymerize OPDA to form PPDA/C composite. The PPDA/C material was centrifuged and washed with water for three times, following with addition of 0.0025 mol FeCl<sub>3</sub> and ultrasonically dispersion. The PPDA/Fe-salt was dried at -45 °C to get the PPDA/Fe-salt hybrid powder. The calcinations procedure was the same as that of Fe-N<sub>x</sub>/C-1.

### Pt/C

Commercial Pt/C (20 wt%) was purchased from Tanaka Kinzoku.

### Instrumentations

X-ray absorption near edge structure (XANES) and extended X-ray absorption fine structure (EXAFS) measurements were performed at the hard X-ray beam line BL01B01 at SPring-8, Japan. Transmission-yield spectra were acquired using a double-crystal Si (111) monochromator. X-ray photoelectron spectroscopy (XPS) was conducted using a Kratos Ultra AXIS Spectrometer system equipped with a monochromatic Al-Kα source. N<sub>2</sub> adsorption/desorption isotherm was tested by a Micromeritics ASAP 2020 system (USA). The specific surface area was determined through Brunauer-Emmett-Teller (BET) method.

### Electrochemical characterization

Electrochemical measurements were performed in a bi-potentiostat (Pine Instrument Co.) equipped with a rotating

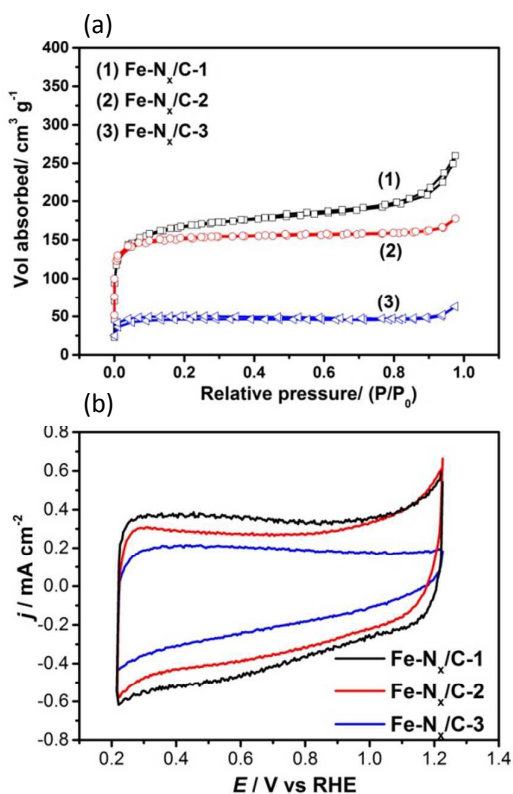


**Figure 2.** (a)  $N_2$  adsorption/desorption isotherm curves of  $Fe-N_x/C$  materials derived from different precursors; (b) The measured CV diagrams of the  $Fe-N_x/C$  catalysts ( $0.4 \text{ mg cm}^{-2}$ ) on glassy carbon electrode (capacitor, 1: 2: 3=1.9: 1.6: 1).

ring-disk electrode (RRDE). A saturated calomel electrode (SCE) was used as a reference electrode and calibrated with respect to a reversible hydrogen electrode (RHE) ( $RHE = SCE^* + 0.244 + 0.591 \times pH$  at  $25^\circ C$ ). A glassy-carbon disk electrode loaded with catalyst/nafion was used as the working electrode and Pt wire was used as the counter electrode. The working electrode was prepared by loading catalyst ink ( $0.4 \text{ mg cm}^{-2}$ ; catalyst to nafion: 4:1) on a glassy carbon electrode. RRDE tests were conducted in an oxygen-gas bubbled KOH and  $K_2SO_4$  ( $0.05 \text{ M}$ ) solution ( $pH 13$ ) at  $25^\circ C$ . A scan rate of  $5 \text{ mV s}^{-1}$  and rotational speed of  $1500 \text{ rpm}$  were used for the ORR activity test. The poised potential of the Pt ring was  $1 \text{ V}$  vs. RHE. The Pt counter electrode was replaced with a carbon stick to exclude the possible contribution of the dissolved Pt species originating from the Pt counter electrode to ORR activity during long-term operation.

## Results and discussion

### Synthesis of $Fe-N_x/C$ catalysts

Figure 1 shows the synthetic route for the  $Fe-N_x/C$  material. First,  $FeCl_3$  solution was added to a mixture of *o*-phenylenediamine (OPDA) and carbon particles to form an  $Fe-OPDA$ -complex/C suspension (step 1). Then, polymerization of  $Fe-OPDA$  to  $Fe-PPDA$  was carried out by adding  $(NH_4)_2S_2O_8$  (step 2). Notably, the oxidative polymerization process decreases the local pH. As the amine-ligand in OPDA and PPDA has higher

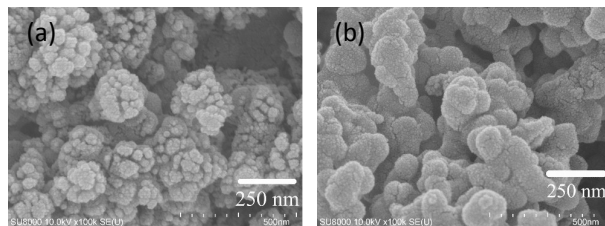


**Figure 3.** SEM images of a)  $Fe-N_x/C-1$  and b)  $Fe-N_x/C-2$  catalysts.

affinity to protons than to  $Fe^{3+}$ ,  $Fe^{3+}$  is released during polymerization.<sup>29</sup> Therefore, we added  $NaHCO_3$  at step-2 as a neutralizer to ensure that the density of coordinated  $Fe-N_x$  in  $Fe-PPDA$  was higher, which was an essential aspect of this work. As the oxidation of  $1 \text{ mol}$  OPDA released  $2 \text{ mol}$  protons, the mole ratios of OPDA and  $NaHCO_3$  were controlled at 1:2. It was confirmed that the pH values were unchanged before and after  $Fe-PPDA$  synthesis in the presence of  $NaHCO_3$ , indicating that the generated protons had been removed via the following reaction:  $HCO_3^- + H^+ \rightarrow CO_2 + H_2O$ , as expected. It should also be noted that the evolved  $CO_2$  gas bubbles can mechanically disrupt the aggregated  $Fe-PPDA$  polymers and decrease the particle size of  $Fe-PPDA$ ,<sup>30</sup> which was effective for increasing the surface area of  $Fe-PPDA$  polymer and final pyrolyzed materials (Figure 2, S1). Hereafter,  $Fe-PPDA$  polymers synthesized in the presence and absence of  $NaHCO_3$  addition are denoted  $Fe-PPDA-1$  and  $Fe-PPDA-2$ , respectively. The resulting product was washed with distilled water three times. The last step was pyrolysis of  $Fe-PPDA$  to form  $Fe-N_x/C$  (step 3), which was treated with concentrated HCl solution to remove impurities before characterization. The pyrolyzed  $Fe-PPDA-1$  and  $Fe-PPDA-2$  were denoted  $Fe-N_x/C-1$  and  $Fe-N_x/C-2$ , respectively.

### Physicochemical characterization

Their morphologies  $Fe-N_x/C-1$  and  $Fe-N_x/C-2$  materials are shown in Figure 3 with observation of scanning electron microscopy (SEM). It was shown that the particle sizes of  $Fe-N_x/C-1$  (Figure 2a) were smaller than that of  $Fe-N_x/C-2$  (Figure 2b), indicating the surface area of  $Fe-N_x/C-1$  was bigger than that of  $Fe-N_x/C-2$ . Low-temperature  $N_2$  absorption/desorption measurements confirmed the bigger Brunauer-Emmett-Teller (BET) surface area (Figure 3a) of  $Fe-N_x/C-1$  ( $621 \text{ m}^2 \text{ g}^{-1}$ ) compared with that of  $Fe-N_x/C-2$  ( $512 \text{ m}^2 \text{ g}^{-1}$ ). It meant that addition of  $NaHCO_3$  played the roles not only for proton neutralization but also for generating  $CO_2$  gas bubbles to break the aggregated polymer, resulting in the higher surface area of  $Fe-N_x/C$  sample. The big difference of BET surface area between  $Fe-PPDA-1$  polymer ( $13.5 \text{ m}^2 \text{ g}^{-1}$ ) and  $Fe-N_x/C-1$  ( $621 \text{ m}^2 \text{ g}^{-1}$ ) indicated that partial elements were removed from polymer during pyrolysis and acidic treatment, and the pyrolyzed sample had highly porous structure. In another words, bulk of polymer was evolved to be surface of  $Fe-N_x/C$  material after pyrolysis treatment. The BET surface area of  $Fe-N_x/C-1$  was over 20 times higher than that of  $Fe-N_x/C-3$  ( $22.8 \text{ m}^2 \text{ g}^{-1}$ ), indicating the effective BET surface area of  $Fe-N_x/C$  was highly promoted by using the iron-coordinated polymer

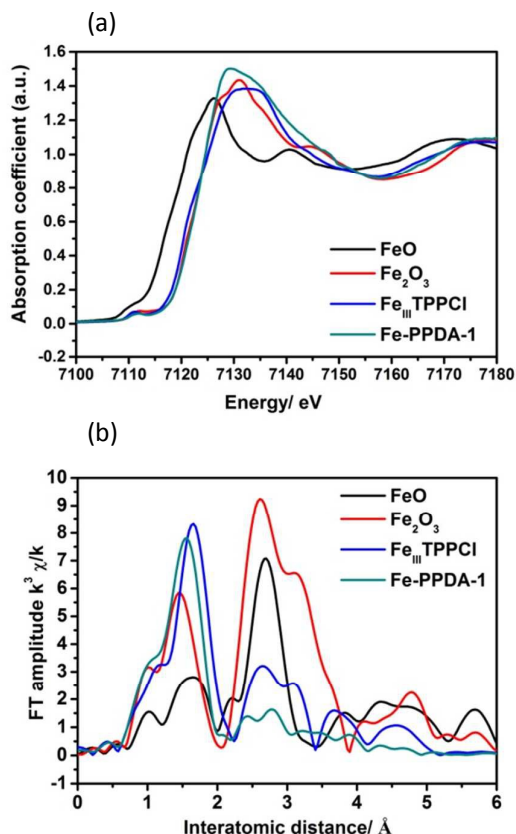


**Figure 4** (a) Normalized Fe K-edge XANES spectra and (b) radial distribution functions of Fourier-transform  $k^3$ -weighted Fe K-edge EXAFS for Fe-PPDA-1 polymer. FeO, Fe<sub>2</sub>O<sub>3</sub> and Fe(III) tetraphenylporphyrin chloride (Fe<sub>III</sub>TPPCI) were used as references.

precursor with porous structure compared to that of physical mixture of iron/polymer precursors.

We investigated whether the Fe-PPDA-1 precursor prepared in the presence of NaHCO<sub>3</sub> possessed the desired structure. The Fe concentration in the Fe-PPDA polymer was determined by surface elemental analysis using X-ray photoelectron spectroscopy (XPS). As shown in Table 1, the Fe concentration in Fe-PPDA-1 was 3.1 mol%, which was much greater than that of Fe-PPDA-2 (0.2 mol%) prepared without NaHCO<sub>3</sub>. The big

	Fe-PPDA-1 mol. %	Fe-PPDA-2 mol. %	Fe-N <sub>x</sub> /C-1 mol. %	Fe-N <sub>x</sub> /C-2 mol. %	Fe-N <sub>x</sub> /C-3 mol. %
C (mol%)	53.7%	62.0%	92.3%	94.5%	91.0%
N (mol%)	23.2%	23.8%	4.8%	3.5%	4.6%
O (mol%)	14.5%	11.2%	1.8%	1.4%	4.0%
S (mol%)	2.6%	2.3%	0.3%	0.1%	0.1%
Cl (mol%)	2.9%	0.6%	0.2%	0.0%	0.0%
Fe (mol%)	3.1%	0.2%	0.6%	0.1%	0.3%

**Table 1** Surface elemental contents of Fe-N<sub>x</sub>/C materials derived from different precursors.

difference of iron-species concentration was also clearly demonstrated from the XPS spectra (Figure S2). The valence states of Fe and Fe-N coordination structure in the bulk of Fe-PPDA-1 polymer were confirmed by X-ray absorption near edge structure (XANES) and extended X-ray absorption fine structure (EXAFS) measurement as shown in Figures 4. In the normalized XANES spectra (Figure 4a), the Fe K-edge position of Fe-PPDA-1 agreed well with those of Fe(III) tetraphenylporphyrin chloride (Fe<sub>III</sub>TPPCI) and Fe<sub>2</sub>O<sub>3</sub>, indicating that the Fe<sup>3+</sup> valence state was dominant in Fe-PPDA-1. The Fourier transform of  $k^3$ -weighted EXAFS oscillations for Fe-PPDA-1 is shown in Figure 4b. Two peaks were dominant in the reference Fe<sub>2</sub>O<sub>3</sub>/FeO, and the corresponding peak at around 1.5 Å/1.65 Å was assigned to the first Fe-O bond, while the peak between 2 and 3.5 Å was attributed to the Fe-Fe bond. In contrast to the spectra of iron oxide, only one peak at 1.58 Å was dominant, demonstrating a very low content of neighboring Fe-Fe species in Fe-PPDA-1.<sup>31</sup> Combination with the above results, as well as the similarity to the spectrum of Fe<sub>III</sub>TPPCI (radius 1.64 Å), the peak at 1.58 Å was assigned to the Fe-N bond in the Fe-PPDA-1 polymer. The minor difference in the radius (1.64 Å vs 1.58 Å) was possibly ascribed to the distorted/flexible square-structure of the Fe-N bond in the polymer. The peak intensity of the Fe-N bond (7.8) in Fe-PPDA-1 was close to that of Fe<sub>III</sub>TPPCI (8.2), which indicated the

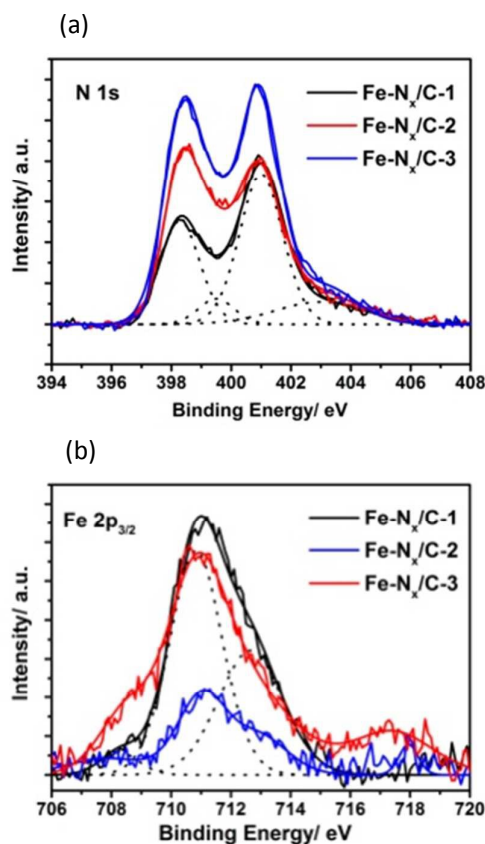


**Figure 5** XPS (a) N 1s and (b) Fe 2p<sub>3/2</sub> spectra of different Fe-N<sub>x</sub>/C materials.

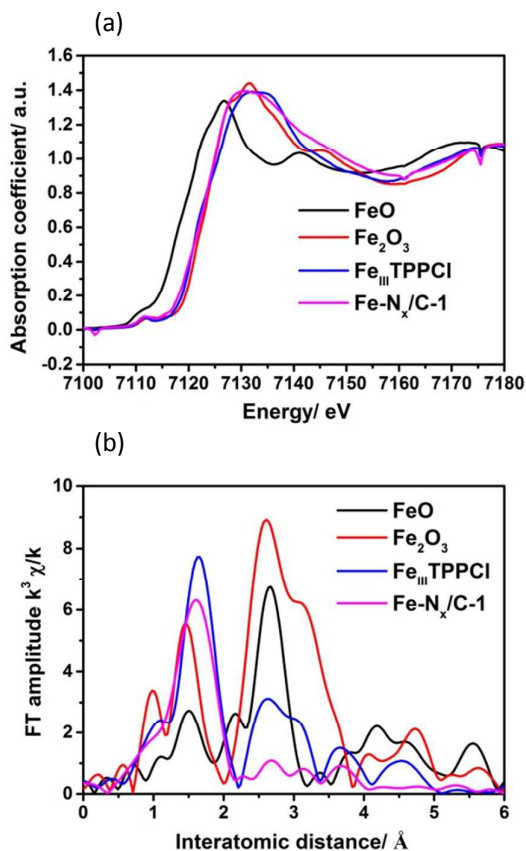


**Figure 6** (a) The normalized XANES spectra at Fe K-edge and (b) Radial distribution functions of Fourier-transformed  $k^3$ -weighted Fe K-edge EXAFS for Fe-N<sub>x</sub>/C-1 materials. FeO, Fe<sub>2</sub>O<sub>3</sub>, Fe<sup>III</sup> tetraphenylporphyrin chloride (Fe<sup>III</sup>TPPCL) were taken as references.

quasi-four/four N coordinated Fe<sup>3+</sup> in Fe-PPDA-1.<sup>31</sup>

Next, we characterized the elemental compositions and contents of Fe-N<sub>x</sub>/C-1 and Fe-N<sub>x</sub>/C-2, obtained by pyrolyzing Fe-PPDA-1 and Fe-PPDA-2, respectively. Figure 5 shows the XPS N 1s and Fe 2p<sub>3/2</sub> spectra of Fe-N<sub>x</sub>/C-1 and Fe-N<sub>x</sub>/C-2. The N 1s peak positions corresponding to pyridinic-N (398.5 eV), pyrrolic-N (399.5 eV), quaternary-N (400.8 eV) and quaternary-N<sup>+</sup>-O<sup>-</sup> (403.1 eV) were close, indicating the similarity in the type of N-species.<sup>18</sup> A big difference was detected in the ratios of N-species calculated from the deconvoluted N 1s spectra (Figure 5a), in which the ratio of quaternary-N species (>60% in total N species) in Fe-N<sub>x</sub>/C-1 was much greater than that in Fe-N<sub>x</sub>/C-2 (<40%). Quaternary-N was the result of in-plane doping, and Fe-N<sub>x</sub> species acted as graphitization catalysts to induce N-atoms preferentially doping into carbon plane rather than at the edges of graphene layer. The higher Fe content in Fe-PPDA-1 resulted in higher ratio of quaternary-N to pyridinic-N compared with that of Fe-PPDA-2.<sup>21</sup> In the XPS Fe 2p<sub>3/2</sub> spectra (Figure 5b), both Fe<sup>2+</sup> (710.9 eV) and Fe<sup>3+</sup> (712.9 eV) were detected in the Fe-N<sub>x</sub>/C samples.<sup>18</sup> Table 1 also summarizes the elemental contents of the Fe-N<sub>x</sub>/C materials. Similar to the higher concentration of N-coordinated Fe

species in Fe-PPDA-1, the Fe content in Fe-N<sub>x</sub>/C-1 (0.6 mol%) was much greater than in Fe-N<sub>x</sub>/C-2 (0.1 mol%).

The Fe coordination structure and valence state in Fe-N<sub>x</sub>/C-1 were characterized by XANES and EXAFS measurements (Figure 6). In the normalized Fe K-edge XANES spectra (Figure 6a), the Fe K-edge position of Fe-N<sub>x</sub>/C-1 was between those of Fe<sup>3+</sup> (references: Fe<sub>2</sub>O<sub>3</sub> and Fe<sup>III</sup>TPPCL) and Fe<sup>2+</sup> (reference: FeO), indicating that both Fe<sup>3+</sup> and Fe<sup>2+</sup> valence states existed. This was consistent with the results observed in XPS Fe 2p<sub>3/2</sub> spectra. The Fourier transform of the K<sup>3</sup>-weighted EXAFS oscillations for Fe-N<sub>x</sub>/C-1 is shown in Figure 6b. In contrast to the spectrum of iron oxide, only one peak at 1.63 Å was dominant, which demonstrated that the content of neighboring Fe-Fe species was very low and that no Fe oxide or metal species existed in Fe-N<sub>x</sub>/C-1. It indicated that mononuclear Fe species were well dispersed on the surface and bulk of Fe-N<sub>x</sub>/C-1, which was possibly important for efficient ORR catalysts. The spectra were similar to those of Fe<sup>III</sup>TPPCL (radius 1.64 Å), and thus, the peak at 1.63 Å can possibly be assigned to the Fe-N bond.<sup>31</sup> Although the possibility of an O-Fe-N structure cannot be ruled out, the dominant Fe species was assumed to be the N-coordinated Fe units. This was due to the fact that only Fe-N units exist in the Fe-PPDA-1 precursor, as well as the high nitrogen content (N=4.8%) of Fe-N<sub>x</sub>/C-1 based on XPS analysis. The calculated coordination number, based on the peak intensity of Fe-N<sub>x</sub>/C-1 (6.3) was approx. 3.3 with respect to the reference compound, Fe<sup>III</sup>TPPCL (intensity, 7.7 Å).<sup>31</sup> Taken together, these results demonstrated that highly concentrated and mononuclear Fe-N<sub>x</sub> units existed in the Fe-N<sub>x</sub>/C-1 sample.

### Electrochemical characterization

Next, the ORR activity of Fe-N<sub>x</sub>/C-1 was examined. Figure 7a shows the ORR polarization curves of Fe-N<sub>x</sub>/C-1, Fe-N<sub>x</sub>/C-2, and Pt/C (20 wt%), measured on a rotating ring-disk electrode (RRDE) at 1500 rpm in a medium of O<sub>2</sub> saturated KOH (pH13). A material prepared from a pyrolyzed hybrid, PPDA/Fe-salt (Fe-N<sub>x</sub>/C-3), was also evaluated as a reference sample. The background capacitive current was corrected (Figure S3). As shown in Figure 7a, the ORR onset potential ( $E_{\text{onset}}$ ) and half-wave potential ( $E_{1/2}$ ) of Fe-N<sub>x</sub>/C-1 (1.08 V and 0.92 V) were much greater than the corresponding values of Fe-N<sub>x</sub>/C-2 catalyst (1.00 V and 0.83 V) and commercial Pt/C (20 wt%, 0.08 mg cm<sup>-2</sup> (Pt), 1.02 V and 0.85 V). Additionally, Fe-N<sub>x</sub>/C-1 with a loading amount of 1 mg cm<sup>-2</sup> gave  $E_{\text{onset}}$  and  $E_{1/2}$  of 1.11 V and 0.92 V, respectively. The ORR activity of Fe-N<sub>x</sub>/C-1 ( $E_{1/2}$ , 0.92 V) was much better than those of the recently-reported excellent Fe-N<sub>x</sub>/C catalysts under the similar condition<sup>17</sup>, such as N-Fe-CNT/CNP materials ( $E_{1/2}$ , 0.87 V),<sup>17</sup> FePhen@MOF-ArNH<sub>3</sub> ( $E_{1/2}$ , 0.86 V),<sup>32</sup> Fe/ANT/C ( $E_{1/2}$ , 0.82 V),<sup>33</sup> and so on.<sup>34</sup> Its' ORR activity was also better than those of the excellent metal-free carbon materials, such as nitrogen-doped carbon nanotube array,<sup>6</sup> N-doped graphene,<sup>7</sup> B,N-co-doped carbon nanotube array,<sup>35</sup> and so on.<sup>17, 32-34</sup>

Although the electrochemically active surface area (EASA) of Fe-N<sub>x</sub>/C-1 was increased (1.2 times) compared with that of Fe-N<sub>x</sub>/C-2 due to the enhancement of BET surface area (Figure

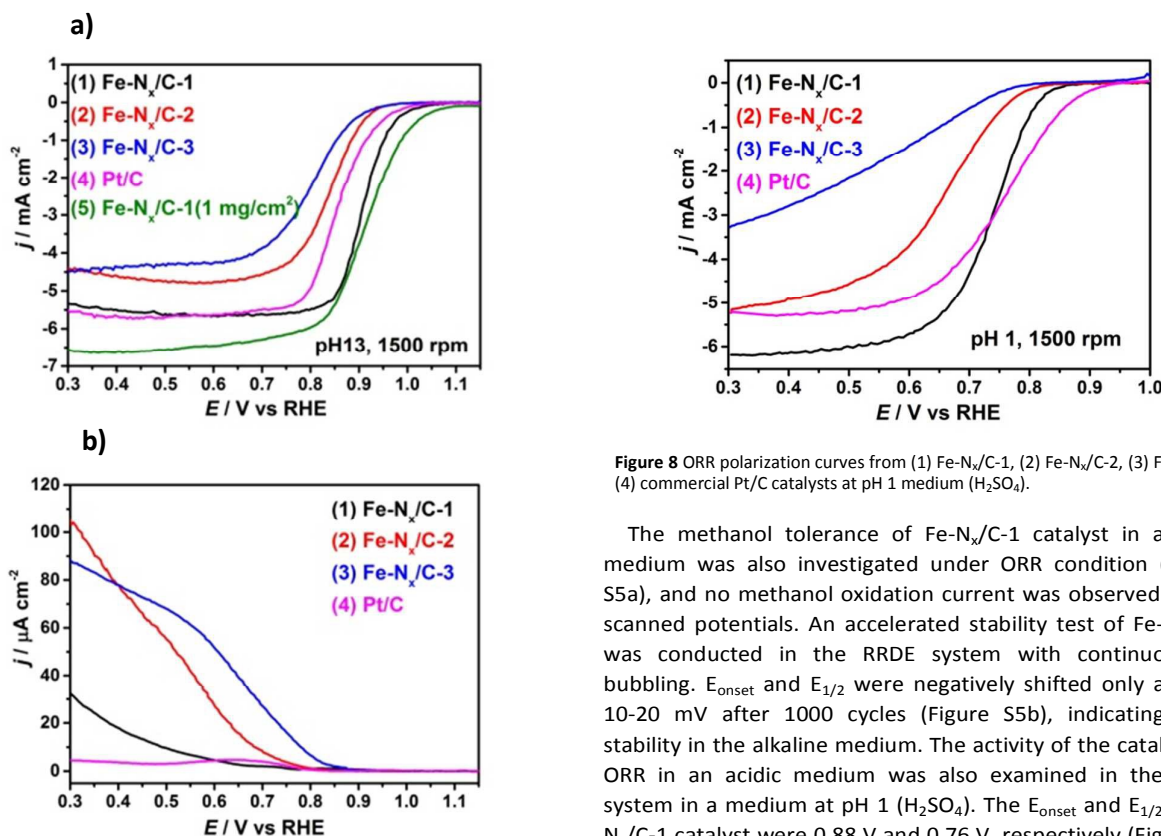


**Figure 8** ORR polarization curves from (1) Fe-N<sub>x</sub>/C-1, (2) Fe-N<sub>x</sub>/C-2, (3) Fe-N<sub>x</sub>/C-3, (4) commercial Pt/C catalysts at pH 1 medium (H<sub>2</sub>SO<sub>4</sub>).

**Figure 7** (a) ORR polarization curves and (b) detected H<sub>2</sub>O<sub>2</sub> production currents from (1) Fe-N<sub>x</sub>/C-1, (2) Fe-N<sub>x</sub>/C-2, (3) Fe-N<sub>x</sub>/C-3, (4) commercial Pt/C catalysts with a loading amount of 0.4 mg cm<sup>-2</sup>, (5) Fe-N<sub>x</sub>/C-1 with the loading amount of 1 mg cm<sup>-2</sup> (pH 13).

2b), the difference in the EASA value was not the only reason for the higher activity of Fe-N<sub>x</sub>/C-1. RRDE experiments revealed that H<sub>2</sub>O<sub>2</sub> production by Fe-N<sub>x</sub>/C-1 was lower than that of Fe-N<sub>x</sub>/C-2 (Fig. 7b). The electron transfer numbers ( $n$ ) (Figure S4) were calculated based on the ratio of disk and ring current in RRDE system according to the equation:  $n = I_d / (I_d + I_r / N)$ , where  $I_d$  and  $I_r$  are the kinetic currents from disk and ring, respectively, and  $N$  is the collection efficiency (0.19). The generated H<sub>2</sub>O<sub>2</sub> oxidative current of Fe-N<sub>x</sub>/C-1 was very low from 1.0 V to 0.6 V, which was similar to that of commercial Pt/C. The calculated electron transfer number at 0.7 V for Fe-N<sub>x</sub>/C-1 was 3.99, similar to that of Pt/C (3.98). The H<sub>2</sub>O<sub>2</sub> oxidative currents from Fe-N<sub>x</sub>/C-2 were greater than that of Fe-N<sub>x</sub>/C-1, and the calculated electron transfer number at 0.7 V was 3.95. Compared with those of Fe-N<sub>x</sub>/C-2, the higher diffusion current density,  $E_{\text{onset}}$  and  $E_{1/2}$  values should be ascribed to higher EASA and active site density of Fe-N<sub>x</sub>/C-1. The low ORR activity of Fe-N<sub>x</sub>/C-3 was possibly ascribed to the low EASA and concentration of active site species, which was consistent to reported results that hybrid of FeCl<sub>3</sub>/PPDA was used as the precursor.<sup>36</sup> The above results indicate that Fe-N<sub>x</sub>/C-1 possessed superior ORR activity and selectivity over those of Fe-N<sub>x</sub>/C-2 and Fe-N<sub>x</sub>/C-3 catalysts, even better than commercial Pt/C in an alkaline medium.

The methanol tolerance of Fe-N<sub>x</sub>/C-1 catalyst in alkaline medium was also investigated under ORR condition (Figure S5a), and no methanol oxidation current was observed at the scanned potentials. An accelerated stability test of Fe-N<sub>x</sub>/C-1 was conducted in the RRDE system with continuous O<sub>2</sub> bubbling.  $E_{\text{onset}}$  and  $E_{1/2}$  were negatively shifted only approx. 10-20 mV after 1000 cycles (Figure S5b), indicating good stability in the alkaline medium. The activity of the catalyst for ORR in an acidic medium was also examined in the RRDE system in a medium at pH 1 (H<sub>2</sub>SO<sub>4</sub>). The  $E_{\text{onset}}$  and  $E_{1/2}$  of Fe-N<sub>x</sub>/C-1 catalyst were 0.88 V and 0.76 V, respectively (Figure 8), much better than those of Fe-N<sub>x</sub>/C-2 and Fe-N<sub>x</sub>/C-3, which highlighted the effect of high content of Fe-N<sub>x</sub> species on ORR activity under different pH condition. The ORR  $E_{1/2}$  in pH1 medium was also comparable to that of commercial Pt/C (20 wt Pt%) catalysts (0.78 V), indicating the advanced ORR activity of Fe-N<sub>x</sub>/C materials. In addition, the ORR stability of Fe-N<sub>x</sub>/C in acidic media was checked and it showed slightly decreased after cycling 500 times (Figure S6). One of the possible reason for the decreased activity was ascribed the loss of Fe-N<sub>x</sub> active sites in acidic environment, which was discussed in previous reports.<sup>21, 34</sup>

#### ORR active site

Fe-N<sub>x</sub> species in polymer have two functions for the formation of Fe-N<sub>x</sub>/C materials as ORR catalysts: the one is the graphitization catalyst to form graphene structure, which is effective to modulate the ratio of quaternary-N to pyridinic-N in carbon matrix;<sup>21, 25</sup> the other is the precursor to form Fe-N<sub>x</sub> species.<sup>24, 37</sup> It was well recognized the effect and importance of N-species and Fe-N<sub>x</sub> species on the ORR activity of Fe-N<sub>x</sub>/C materials,<sup>6, 7, 21</sup> and both were proposed as the possible candidates as catalytic active centers. Comparing the samples of Fe-N<sub>x</sub>/C-1 and Fe-N<sub>x</sub>/C-2, their large difference of ORR activities and selectivity should correlate with N-coordinated Fe concentration (0.6 mol% vs 0.1 mol%) and the ratio of quaternary-N to pyridinic-N. Although we cannot conclude which one played the dominant role, the mono-dispersed Fe-N<sub>4</sub> with high concentration in the polymer precursor was revealed to be essentially important to obtain the Fe-N<sub>x</sub>/C with

both dense Fe-N<sub>x</sub> species and high ratio of quaternary-N to pyridinic-N. Synthesis of Fe-coordinated polymer in present study is the key to obtain the extraordinary ORR activity of Fe-N<sub>x</sub>/C materials.

## Conclusions

In summary, we synthesized iron-coordinated aromatic polymer, Fe-PPDA-1, by polymerization of Fe-OPDA complex in the presence sodium carbonate, which was taken as the key factor in retaining the Fe-N coordination units in the Fe-PPDA-1 polymer, and increasing surface area by evolved CO<sub>2</sub> gas breaking the aggregated polymer. The dense and mono-dispersed Fe-N species, modulated carbon structure, and high surface area were thought to be the reasons for the efficient ORR activity of Fe-N<sub>x</sub>/C catalyst. The present study provides new insights of bottom-up synthesis method to obtain efficient M-N<sub>x</sub>/C catalysts from rational design of catalyst precursors.

## Acknowledgements

Synchrotron radiation experiments were performed at the BL01B1 beam line of SPring-8 with the approval of the Japan Synchrotron Radiation Research Institute (JASRI; Proposals Nos 2015A1302, 2014B1252 and 2013B1123). We thank Dr. T. Ina for his technical support during XAFS measurements at SPring-8 and Dr. Zhongqun Tian for valuable discussions at Xiamen University, China.

## Notes and references

- 1 J. Suntivich, H. A. Gasteiger, N. Yabuuchi, H. Nakanishi, J. B. Goodenough and Y. Shao-Horn, *Nat. Chem.*, 2011, **3**, 546-550.<sup>1</sup>
- 2 Y. Y. Liang, H. L. Wang, J. G. Zhou, Y. G. Li, J. Wang, T. Regier and H. J. Dai, *J. Am. Chem. Soc.*, 2012, **134**, 3517-3523.<sup>1</sup>
- 3 M. R. Gao, J. Jiang and S. H. Yu, *Small*, 2012, **8**, 13-27.<sup>1</sup>
- 4 G. Yang, W. Choi, X. Pu and C. Yu, *Energy Environ. Sci.*, 2015, **8**, 1799-1807.<sup>1</sup>
- 5 H. L. Wang, Y. Y. Liang, Y. G. Li and H. J. Dai, *Angew. Chem., Int. Ed.*, 2011, **50**, 10969-10972.<sup>1</sup>
- 6 K. P. Gong, F. Du, Z. H. Xia, M. Durstock and L. M. Dai, *Science*, 2009, **323**, 760-764.<sup>1</sup>
- 7 L. T. Qu, Y. Liu, J. B. Baek and L. M. Dai, *Acs Nano*, 2010, **4**, 1321-1326.<sup>1</sup>
- 8 S. Wang, S. M. Dong, J. Wang, L. X. Zhang, P. X. Han, C. J. Zhang, X. G. Wang, K. J. Zhang, Z. G. Lan and G. L. Cui, *J. Mater. Chem.*, 2012, **22**, 21051-21056.<sup>1</sup>
- 9 K. Parvez, S. B. Yang, Y. Hernandez, A. Winter, A. Turchanin, X. L. Feng and K. Mullen, *Acs Nano*, 2012, **6**, 9541-9550.<sup>1</sup>
- 10 S. L. Zhao, H. J. Yin, L. Du, L. C. He, K. Zhao, L. Chang, G. P. Yin, H. J. Zhao, S. Q. Liu and Z. Y. Tang, *Acs Nano*, 2014, **8**, 12660-12668.<sup>1</sup>
- 11 M. K. Debe, *Nature*, 2012, **486**, 43-51.<sup>1</sup>
- 12 A. Holewinski, J. C. Idrobo and S. Linic, *Nat. Chem.*, 2014, **6**, 828-834.<sup>1</sup>

- 13 F. Calle-Vallejo, M. T. M. Koper and A. S. Bandarenka, *Chem. Soc. Rev.*, 2013, **42**, 5210-5230.<sup>1</sup>
- 14 W. Cheng and R. G. Compton, *Angew. Chem., Int. Ed.*, 2015, **54**, 7082-7085.<sup>1</sup>
- 15 Z. L. Li, G. L. Li, L. H. Jiang, J. L. Li, G. Q. Sun, C. G. Xia and F. W. Li, *Angew. Chem., Int. Ed.*, 2015, **54**, 1494-1498.<sup>1</sup>
- 16 M. S. Faber and S. Jin, *Energy Environ. Sci.*, 2014, **7**, 3519-3542.<sup>1</sup>
- 17 H. T. Chung, J. H. Won and P. Zelenay, *Nat. Commun.*, 2013, **4**:1922,<sup>1</sup>
- 18 Y. Zhao, K. Watanabe and K. Hashimoto, *J. Am. Chem. Soc.*, 2012, **134**, 19528-19531.<sup>1</sup>
- 19 I. Hijazi, T. Bourgeteau, R. Cornut, A. Morozan, A. Filoramo, J. Leroy, V. Derycke, B. Jouselme and S. Campidelli, *J. Am. Chem. Soc.*, 2014, **136**, 6348-6354.<sup>1</sup>
- 20 J. Liu, X. J. Sun, P. Song, Y. W. Zhang, W. Xing and W. L. Xu, *Adv. Mater.*, 2013, **25**, 6879-6883.<sup>1</sup>
- 21 G. Wu and P. Zelenay, *Acc. Chem. Res.*, 2013, **46**, 1878-1889.<sup>1</sup>
- 22 X. W. Liu, W. W. Li and H. Q. Yu, *Chem. Soc. Rev.*, 2014, **43**, 7718-7745.<sup>1</sup>
- 23 S. Gupta, D. Tryk, I. Bae, W. Aldred and E. Yeager, *J. Appl. Electrochem.*, 1989, **19**, 19-27.<sup>1</sup>
- 24 Q. Wang, Z. Y. Zhou, Y. J. Lai, Y. You, J. G. Liu, X. L. Wu, E. Terefe, C. Chen, L. Song, M. Rauf, N. Tian and S. G. Sun, *J. Am. Chem. Soc.*, 2014, **136**, 10882-10885.<sup>1</sup>
- 25 G. Wu, K. L. More, C. M. Johnston and P. Zelenay, *Science*, 2011, **332**, 443-447.<sup>1</sup>
- 26 C. Walter, K. Kummer, D. Vyalikh, V. Bruser, A. Quade and K. D. Weltmann, *J. Electrochem. Soc.*, 2012, **159**, F560-F569.<sup>1</sup>
- 27 H. S. Liu, Z. Shi, J. L. Zhang, L. Zhang and J. J. Zhang, *J. Mater. Chem.*, 2009, **19**, 468-470.<sup>1</sup>
- 28 S. G. Wang, Z. T. Cui and M. H. Cao, *Chem. Eur. J.*, 2015, **21**, 2165-2172.<sup>1</sup>
- 29 R. A. Periana, D. J. Taube, S. Gamble, H. Taube, T. Satoh and H. Fujii, *Science*, 1998, **280**, 560-564.<sup>1</sup>
- 30 Y. Zhao, K. Kamiya, K. Hashimoto and S. Nakanishi, *J. Am. Chem. Soc.*, 2015, **137**, 110-113.<sup>1</sup>
- 31 J. J. Wu, D. Zhang, H. Niwa, Y. Harada, M. Oshima, H. Ofuchi, Y. Nabae, T. Okajima and T. Ohsaka, *Langmuir*, 2015, **31**, 5529-5536.<sup>1</sup>
- 32 K. Strickland, M. W. Elise, Q. Y. Jia, U. Tylus, N. Ramaswamy, W. T. Liang, M. T. Sougrati, F. Jaouen and S. Mukerjee, *Nat. Commun.*, 2015, **6**:7343<sup>1</sup>
- 33 Y. Q. Chang, F. Hong, C. X. He, Q. L. Zhang and J. H. Liu, *Adv. Mater.*, 2013, **25**, 4794-4799.<sup>1</sup>
- 34 L. M. Dai, Y. H. Xue, L. T. Qu, H. J. Choi and J. B. Baek, *Chem. Rev.*, 2015, **115**, 4823-4892.<sup>1</sup>
- 35 S. Y. Wang, E. Iyyamperumal, A. Roy, Y. H. Xue, D. S. Yu and L. M. Dai, *Angew. Chem., Int. Ed.*, 2011, **50**, 11756-11760.<sup>1</sup>
- 36 Y. S. Zhu, B. S. Zhang, X. Liu, D. W. Wang and D. S. Su, *Angew. Chem., Int. Ed.*, 2014, **53**, 10673-10677.<sup>1</sup>
- 37 W. M. Li, J. Wu, D. C. Higgins, J. Y. Choi and Z. W. Chen, *Acs Catalysis*, 2012, **2**, 2761-2768.<sup>1</sup>

**The table of contents**

Iron-coordinated polymer (Fe(III)-poly(o-phenylenediamine)) produced iron/nitrogen co-doped carbon electrocatalyst demonstrates highly efficient oxygen reduction reaction activity in both alkaline and acidic media.

